Carbohydrate Polymers 165 (2017) 123–131

Contents lists available at ScienceDirect

Carbohydrate Polymers

journal homepage: www.elsevier.com/locate/carbpol

Solid polymer electrolyte production from 2-hydroxyethyl cellulose: Effect of ammonium nitrate composition on its structural properties

M.N. Hafiza, M.I.N. Isa*

Advanced Materials Team, Ionic State Analysis (ISA) Laboratory, School of Fundamental Science, Universiti Malaysia Terengganu, 21030 Kuala Nerus, Terengganu Darul Iman, Malaysia

ARTICLE INFO

Article history:
Received 20 October 2016
Received in revised form 28 January 2017
Accepted 10 February 2017
Available online 14 February 2017

Keywords:
2-hydroxyethyl cellulose
Ammonium nitrate
Solid polymer electrolyte
Amorphous nature
Complexation
Ionic conductivity

ABSTRACT

Addition of doping materials can possibly enhance the ionic conduction of solid polymer electrolyte (SPE). In this work, a new SPE using 2-hydroxyethyl cellulose (2-HEC) incorporated with different ammonium nitrate (NH_4NO_3) composition was prepared via solution casting method. Studies of structural properties were conducted to correlate the ionic conductivity of 2-HEC—NH_4NO_3 SPE using X-ray diffraction (XRD) and Fourier transform infrared (FTIR) spectroscopy. Encouraging result was obtained as the ionic conductivity increased about two orders of magnitude upon addition of 12 wt% of NH_4NO_3. XRD analysis shows the most amorphous SPE was obtained at 12-NH_4NO_3. From FTIR spectra, the interactions between 2-HEC and NH_4NO_3 were observed by the shifts of C—O—H peak from 1355 cm^{-1} to 1330 cm^{-1} and the presence of new N—H peak in the O—H region. The spectrum has been validated theoretically using Gaussian software. The results obtained from this study corroborate that the complexes of 2-HEC and NH_4NO_3 responsible to promote the ionic conductivity to the higher value.

1. Introduction

Polymer has been used for over fifty-years in industry as electronic insulators, adhesives and biomedical materials (Allen, 1986; Isa & Samsudin, 2016; Pethrick, 1986). The discovery of ionic conductive polymer in 1975 by Wright led in development of solid polymer electrolyte (SPE) for more than 15 years and carefully studied when Armand proposed to implement the electrolyte in batteries in 1978 (Isa & Samsudin, 2016; Murata, 1995; Murata, Izuchi, & Yoshihisa, 2000; Przyłuski & Wieczorek, 1989; Sohaimy & Isa, 2016). In SPE, polymer plays a role as the host for ion migration (Ahmad & Isa, 2016). Natural polymer has been widely studied to replace synthetic polymer in SPE due to high demand for greener technology (Monisha et al., 2017; Ramesh, Shanti, & Morris, 2013; Ramlli & Isa, 2016). Previous studies have also reported that by adopting natural polymer in SPE, it gives out a good performance when utilized in electrochemical devices such as battery (Alias, Chee, & Mohamad, 2014; Samsudin, Lai, & Isa, 2014; Shukur & Kadir, 2015). On top of that, it also reduces the environmental impact and improves the safety of a battery (Liew & Ramesh, 2015; Rudhziah, Rani, Ahmad, Mohamed, & Kaddami, 2015; Samsudin et al., 2014; Shukur & Kadir, 2015).

Among all the natural polymers, cellulose (carbohydrate polymer) is inexhaustible source in nature with approximately 5×10^{11} metric tons produce in a year (Abdel-Halim, 2014; Qiu & Hu, 2013). Moreover, cellulose is non-toxic and biodegradable polymer (Miao et al., 2016). 2-hydroxyethyl cellulose (2-HEC) is one of cellulose derivatives. It has received a great attention from industry and group of researchers as it possess good chemical stability, biocompatible, excellent thickening and stabilizing agent and tendency for adhesion product and film-formation (Abd El-kader & Abu-Abdeen, 2012; Eissa, Khosravi, & Cimecioglu, 2012). Presence of hydroxyethyl group (CH_2—CH_2—OH) in 2-HEC makes it a highly water-soluble carbohydrate (Taghizadeh & Seifi-Aghjekohal, 2015). These advantages enable 2-HEC to be developed as solid polymer electrolyte.

However, the use of natural polymer material in SPE gives relatively low ionic conductivity (Hafiza & Isa, 2014; Pawlicka, Sabadini, Raphael, & Dragunski, 2008; Sudaryanto, Yulianti, & Patimatuzzohrah, 2016). Thus limits the use of SPE in electrochemical devices (Awadhia & Agrawal, 2007). Numerous methods have been employed in order to improve the ionic conductivity of SPE such as blending, copolymerization, incorporation of filler/doping material (Amaral et al., 2015; Bakar, Hafiza, Bashirah, & Isa, 2015; Byrne, Efthimiadis, MacFarlane, & Forsyth, 2004). Recent investiga-

* Corresponding author.
E-mail addresses: ikmarnizam@gmail.com, ikmar_isa@umt.edu.my (M.I.N. Isa).

http://dx.doi.org/10.1016/j.carbpol.2017.02.033
0144-8617/

Table 1
Composition of 2-HEC—NH_4NO_3 SPEs.

Designation (2-HEC + NH_4NO_3)	2-HEC (±0.0001 g)	NH_4NO_3 (wt.%)
0-NH_4NO_3	2.0000	0
4-NH_4NO_3		4
8-NH_4NO_3		8
12-NH_4NO_3		12
16-NH_4NO_3		16
20-NH_4NO_3		20
24-NH_4NO_3		24

tions have showed that the incorporation of doping material is the cheapest and simplest method (Monisha et al., 2017; Sohaimy & Isa, 2016; Voigt & van Wüllen, 2012) which can possibly overcome the mentioned limitation. To date, ammonium salt such as ammonium nitrate, ammonium chloride, ammonium bromide and ammonium iodide is the promising doping material in proton conducting electrolyte system as it provides ions – which is proton (H^+) species, for conduction process. In addition, ammonium salt is also considered as a good proton donor which could endorse the proton conduction through the polymer matrix as well as could promote the ionic conductivity to higher value (Radha, Selvasekarapandian, Karthikeyan, Hema, & Sanjeeviraja, 2013; Salleh, Aziz, Aspanut, & Kadir, 2016).

Despite many researchers done on cellulose-based SPE, there is no report on the interaction of 2-HEC—NH_4NO_3 SPE system. Therefore, the present study embarks on the investigation of NH_4NO_3 effect on the structural properties of 2-HEC SPE by using X-ray diffractometer (XRD) and Fourier transform infrared (FTIR) spectroscopy. XRD analysis is used to determine the amorphous nature of the SPE. The spectra from FTIR analysis are also compared with theoretical analysis of Gaussian 09 quantum mechanical software to confirm the interaction between 2-HEC and NH_4NO_3. The results obtained from this study were used to correlate the structural properties and ionic conductivity of 2-HEC—NH_4NO_3 SPE.

2. Experimental

2.1. Materials

2-hydroxyethyl cellulose (2-HEC) powder with molecular weight of ~90, 000 g/mol and ammonium nitrate (NH_4NO_3) salt with 99.0% purity were purchased from Sigma-Aldrich Inc. All materials were used without any purification.

2.2. SPE preparation

SPEs were prepared via well-known solution casting method with some modification. 2 g of 2-HEC was dissolved in distilled water at room temperature and stirred until complete dissolution. Various amounts of NH_4NO_3 ranging from 4 wt.% to 24 wt.% (interval 4 wt.%) was added into the solution and continuously stirred until the solution turns homogenous with no phase separations. The solution was poured into glass petri dishes and left dried in oven at 50 °C for the SPE to be formed. The SPEs were then kept in desiccator prior to be characterized to remove any residual moisture. The composition of 2-HEC—NH_4NO_3 SPEs is shown in Table 1.

2.3. SPE characterization

2.3.1. Electrical impedance spectroscopy (EIS)

EIS was performed using HIOKI 3532-50 LCR Hi-Tester interfaced to a computer in the frequency ranging between 50 Hz to 1 MHz. The samples were cut into small discs of 2 cm diameter and sandwiched between two stainless steel blocking electrodes under spring pressure. The ionic conductivity, σ was calculated using Eq. (1) below (Ali, Mohamed, & Arof, 1998; Bakar et al., 2015; Hafiza, Bashirah, Bakar, & Isa, 2014).

$$\sigma = \frac{t}{R_b A} \quad (1)$$

From the equation, A (cm^2) is the electrode-electrolyte contact area of SPE and t (cm) is the thickness of SPE. The bulk impedance, R_b was obtained by plotting the negative imaginary impedance, $-Z_i$ versus real part, Z_r of impedance.

2.3.2. X-ray diffraction (XRD)

XRD patterns were measured using Rigaku MiniFlex II diffractometer with CuK_α radiation to determine the nature of SPE formed whether they are crystalline, amorphous or both. The diffraction patterns were scanned at room temperature from 2θ = of 5° to 75° with step of 0.02° and speed of 2.00°/min.

In XRD deconvolution technique, Origin Lab Software was used. The baseline function was applied to the specified region. By assuming Gaussian function, the amorphous and crystalline peaks were deconvoluted and all peaks were ensured to fit the original spectrum. After extracting the peak, the area under the peaks was determined and the degree of crystallinity was calculated using Eq. (2) below (Abdul Rahaman et al., 2014).

$$\chi_c = \frac{A_c}{A_c + A_a} \times 100\% \quad (2)$$

Here, A_c is the area under the peaks representing the total crystalline region and A_a is the area under the peaks representing the total amorphous region.

2.3.3. Fourier transform infrared (FTIR) spectroscopy

FTIR spectroscopy measurement was done using Thermo Nicolet 380 FTIR spectrometer, to determine intermolecular interaction of SPEs. The SPEs were tested by Attenuated Total Reflection (ATR) measurement in the frequency ranging between 650 cm^{-1} to 4000 cm^{-1} with resolution of 4 cm^{-1}.

Prior to curve fitting, the infrared spectra was selected in region from 1500 cm^{-1} to 1200 cm^{-1} and 3800 cm^{-1} to 3000 cm^{-1} for the baseline creation. After the baseline was applied, the spectra was deconvoluted and fitted by a sum of Gaussian function which is adapted from the Origin Lab software. The sum of intensity for all deconvoluted peaks was ensured to fit the original spectrum (Chai & Isa, 2016).

2.3.4. Gaussian analysis software

Gaussian 09 quantum mechanical software package was used to perform the geometry optimization and computation of harmonic vibrational frequency on a large set of molecules. For the present work, the molecular structure of 2-HEC, NH_4NO_3 and 2-HEC—NH_4NO_3 complexes were optimized at theoretical level of DFT/B3LYP using 6–31G (d,p) basic set. One unit of 2-HEC and NH_4NO_3 molecules were used to represent the optimized structure of 2-HEC—NH_4NO_3 complexes. The optimized molecular structure was used in the vibrational frequency calculation at the same level of theory and basic set. The vibrational assignments were obtained using GAUSSVIEW animation program (Ahmad & Isa, 2016; Poiyamozhi, Sundaraganesan, Karabacak, Tanrıverdi, & Kurt, 2012).

3. Results and discussion

3.1. Ionic conductivity analysis

The effect of NH_4NO_3 doping on the ionic conductivity of 2-HEC SPE was evaluated and shown in Fig. 1. Noted from the figure, ionic conductivity increases from $(3.33 \pm 0.05) \times 10^{-6}$ S cm^{-1}

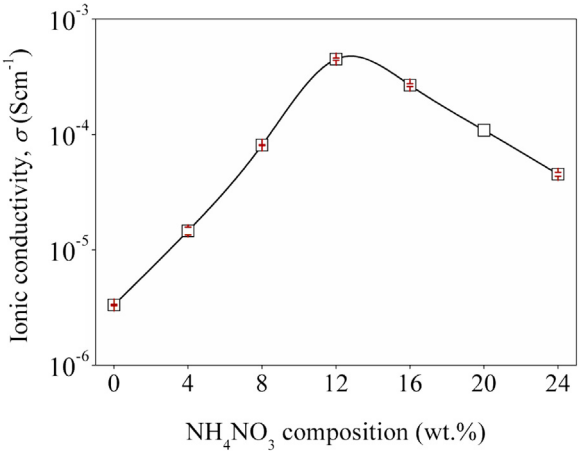

Fig. 1. Ionic conductivity against NH_4NO_3 composition.

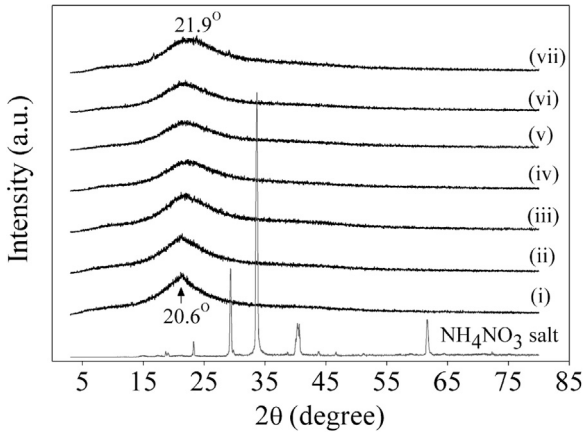

Fig. 2. XRD spectrum for NH_4NO_3 salt, 2-HEC SPE with (i) 0-NH_4NO_3; (ii) 4-NH_4NO_3; (iii) 8-NH_4NO_3; (iv) 12-NH_4NO_3; (v) 16-NH_4NO_3; (vi) 20-NH_4NO_3 and (vii) 24-NH_4NO_3 composition.

to $(1.46 \pm 0.11) \times 10^{-5}$ S cm^{-1} upon addition of NH_4NO_3 and further enhanced to $(4.51 \pm 0.10) \times 10^{-4}$ Scm^{-1} with the addition of 12 wt.% NH_4NO_3. It is noted that the enhancement of ionic conductivity may be attributed by the increasing of amorphous nature of the sample (Ramlli & Isa, 2016). Similarly reported by Ramlli & Isa (2016), it is believed in this system, the increase of amorphousness has promotes the ion transport.

On the other hand, the number of ion dissociation is of another factor that contributes to the ionic conductivity enhancement. The increase in the ionic conductivity can be inferred as being due to the dissociation of NH_4NO_3, more free ions are supplied in the SPE system as the composition of NH_4NO_3 increases similarly found by most polymer-salt systems (Samsudin & Isa, 2014; Shukur & Kadir, 2014; Sim, Yahya, & Arof, 2016). The addition of NH_4NO_3 doping introduces the free cation (NH_4^+) and free anion (NO_3^-) to be dissociated. The dissociated cation occurs when incorporation salt interact with polar group of polymer host. Thus more cations are expected to participate in the ion conduction (Monisha et al., 2017). High degree of ion dissociated promotes the ionic conductivity to higher value. However, at higher NH_4NO_3 composition (above 12 wt.%), the decrease in ionic conductivity can be ascribed to the aggregation of ion cluster, which leads to the formation of overcrowded of ions (Hafiza et al., 2014; Selvasekarapandian, Hema, Kawamura, Kamishima, & Baskaran, 2010) in the polymer-salt system.

The dissociation of salt into free ions could be investigated by the shifting, emergence and/or presence of new peaks from the FTIR spectrum. Herewith, the amorphous nature and interaction of the 2-HEC—NH_4NO_3 SPE is observed and discussed in details to support the above inferences.

3.2. XRD analysis

XRD is a powerful technique to identify the changes in the SPE phases which is available in both crystalline and amorphous region (Abdul Rahaman et al., 2014; Ramesh et al., 2013). In SPE, amorphous material is generally associated with the ability to endorse the ionic motion. It can be interpreted by Hodge et al. (1996) criterion, which establishes a correlation between the intensity of the peak and the degree of crsystallinity (Hodge, Edward, & Simon, 1996; Samsudin, Khairul, & Isa, 2012). Fig. 2 presents the XRD spectra of the studied SPE and NH_4NO_3 salt. From Fig. 2, crystalline peaks of NH_4NO_3 salts located at 23.2°, 29.4°, 33.8°, 40.6° and 61.6°. A broad peak centred at 20.6° indicates amorphous nature of 2-HEC SPE (Fig. 2(i)). However, noticeable changes in XRD pattern occurred after addition of NH_4NO_3. The peak becomes broader and shifts to higher 2θ angle of 21.9° as the effect of NH_4NO_3 composition. The increase in broadness is the evidence of the amorphousness of the SPE (Selvasekarapandian, Hema, Kawamura, Kamishima, & Baskaran, 2010). As deduced earlier, the amorphousness is significantly importance as it imparts more number of vacant oxygen for H^+ ion coordination thus eases the ion transportation through the 2-HEC backbone. The continuous of H^+ ion hopping along the polymer backbone subsequently increase the ionic conductivity (Liew & Ramesh, 2015; Ramesh et al., 2013). The absence of additional peak for sample containing 4 wt.%–24 wt.% of NH_4NO_3 implies a complete dissolution of NH_4NO_3 doping in the 2-HEC polymer matrix (Singh, Jadhav, Majumder, Bhattacharya, & Singh, 2013).

Table 2
A_c, A_a and χ_c of 2-HEC SPE with different NH_4NO_3 composition.

Sample	A_c	A_a	χ_c (%)
0-NH_4NO_3	0.97	11.44	7.85
4-NH_4NO_3	1.05	12.40	7.82
8-NH_4NO_3	0.87	14.76	5.57
12-NH_4NO_3	0.71	15.50	4.35
16-NH_4NO_3	1.40	14.62	8.75
20-NH_4NO_3	1.50	12.29	10.87
24-NH_4NO_3	3.05	12.84	19.18

XRD deconvolution technique (Abdul Rahaman et al., 2014; Fadzallah, Majid, Careem, & Arof, 2014) was used to study the explicit detail on the amorphous nature of the SPE. The XRD deconvolutions of 2-HEC—NH_4NO_3 SPEs are shown in Fig. 3. From Fig. 3, the amorphous peaks are shown by the dotted line whereas the crystalline peaks are shown by the black line in the figure. The peak observed in this study is almost similar to the work done by Trivedi, Nayak, Patil, Tallapragada, and Mishra (2015). The degree of crystallinity of the SPEs was calculated from the ratio of the area of crystallinity peak to the total area of deconvolution peaks by using Eq. (2). By determining the degree of crystallinity, the amorphous degree was obtained since the highest crystallinity value corresponds to the lowest amorphous value.

The area of total crystalline region, area of the total amorphous region and degree of crsytallinity is tabulated in Table 2. Based on Table 2, it is observed that addition of NH_4NO_3 up to 12 wt.% has increased the amorphousness of 2-HEC SPE as results of reduction in degree of crystallinity and consequently, the ionic conductivity increases. Beyond this composition, the amorphous degree is observed to decrease and hence, the ionic conductivity decreases. The results obtained from this study proved that the ionic conductivity of 2-HEC—NH_4NO_3 SPE is affected by the amorphousness

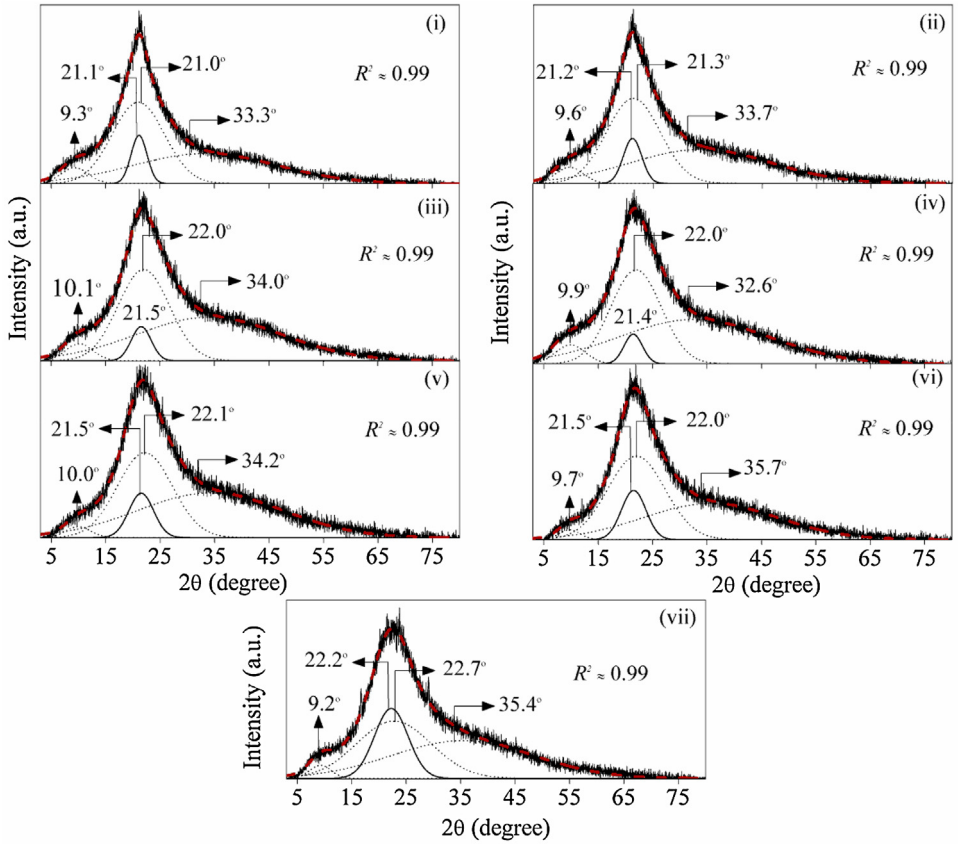

Fig. 3. XRD deconvolution for 2-HEC SPE with (i) 0-NH_4NO_3; (ii) 4-NH_4NO_3; (iii) 8-NH_4NO_3; (iv) 12-NH_4NO_3; (v) 16-NH_4NO_3; (vi) 20-NH_4NO_3 and (vii) 24-NH_4NO_3 composition.

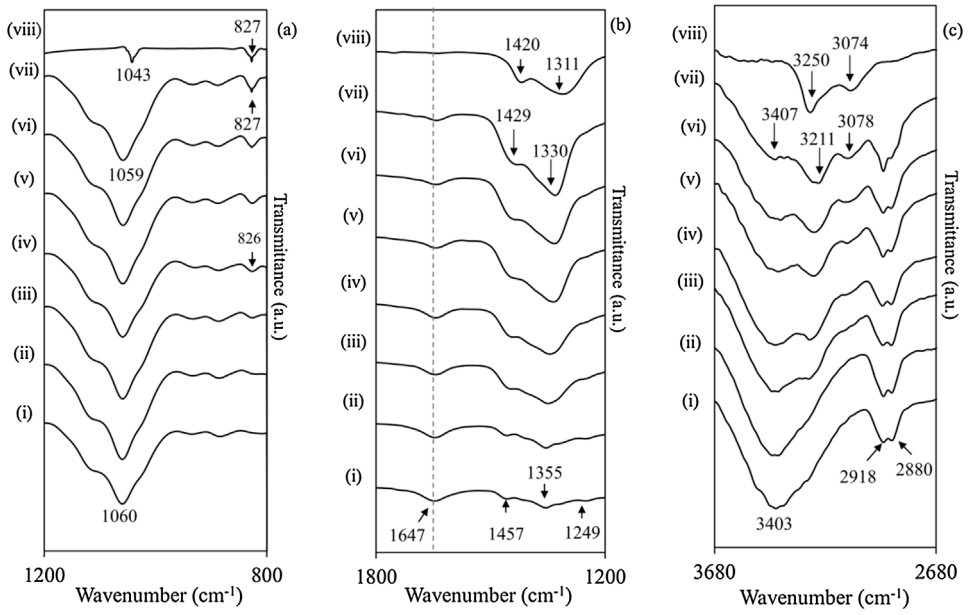

Fig. 4. FTIR spectra for 2-HEC SPE with (i) 0-NH_4NO_3; (ii) 4-NH_4NO_3; (iii) 8-NH_4NO_3; (iv) 12-NH_4NO_3; (v) 16-NH_4NO_3; (vi) 20-NH_4NO_3 and (vii) 24-NH_4NO_3 composition and (viii) NH_4NO_3 salt in the region of a) 1200–800 cm^{-1}, b) 1800–1200 cm^{-1} and c) 3680–2680 cm^{-1}.

of the samples. As mentioned earlier, for this system, it can be concluded that the increase of amorphousness has promotes the ion transport (Ramlli & Isa, 2016). Since the ionic transport of SPE only occurs in amorphous materials, higher dissociation of NH_4NO_3 into free ion and migration of ions through polymer chain which

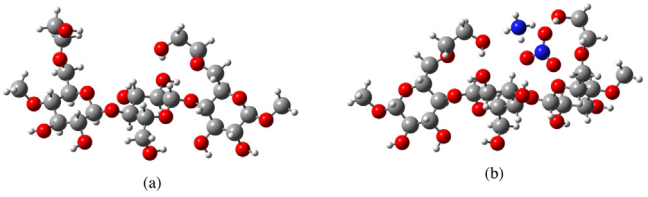

Fig. 5. Molecular structure retrieved from Gaussian software (GaussView 5.0) representation of optimized (a) 2-HEC and (b) 2-HEC—NH_4NO_3 complexes. Dark grey is carbon atom, light grey is hydrogen atom, red is oxygen atom and blue is nitrogen atom. (For interpretation of the references to colour in this figure legend, the reader is referred to the web version of this article.).

effected the ionic conductivity can be further proved from FTIR analysis (Ibrahim, Yassin, Ahmad, & Johan, 2011).

3.3. FTIR analysis

Table 3 lists the vibration modes of 2-HEC powder and NH_4NO_3 salts. For pure 2-HEC, the presence of C—O and C—C vibration modes in region of 1500 cm^{-1}–600 cm^{-1}, displays the characteristic of carbohydrate (Shameli et al., 2012) thus confirmed the structure of 2-HEC. Considerably different wavenumber between experimental and Gaussian calculation may effect from the movement of molecules. Thus, the experiment results for both molecules were acceptable and comparable with the calculated frequency from Gaussian analysis software and tabulated in Table 3. On top of that, the vibrational frequency obtained from Gaussian analysis also shows no imaginary value, indicating that the optimized molecular structure of 2-HEC, NH_4NO_3 and 2-HEC—NH_4NO_3 complexes is stable (Ahmad & Isa, 2016; Monisha et al., 2017).

Deeper understanding of intermolecular interaction between 2-HEC and NH_4NO_3 provide valuable insight over mechanism of ionic conductivity enhancement in SPE. Examination of the shift in absorption position, change in band contours accompanying by the absence/or presence of new peak, give the important structural details for the polymer-salt complexation in FTIR analysis (Shukur, Ithnin, Illias, & Kadir, 2013). In the present work, FTIR analysis has been performed by both experimental and computational method to determine the functional group of non-complexes and complexes 2-HEC—NH_4NO_3 SPE. Figs. 4 and 5 demonstrate the IR-spectrum and the optimized molecular structure of 2-HEC and 2-HEC—NH_4NO_3 complexes respectively, which were obtained from Gaussian analysis software. The spectrums were interpreted into three potential regions, the region were a) 1200–800 cm^{-1}, b) 1800–1200 cm^{-1} and c) 3680–2680 cm^{-1}.

Several noticeable changes were observed in the region of hydroxyl (O—H) band. The O—H bond is highly polar molecules due to the large electronegativity difference between oxygen and hydrogen. This strong dipole is generally give rise to strong absorption in the IR (Silverstein, Webster, & Kiemle, 2005). In polymer-salts/dopant system, cation tends to coordinate with polar molecules for complexation to occur, consequently affecting the vibration of infrared active modes (Shukur & Kadir, 2014). The transporting cation for this study could be NH_4^+ constituent either H^+ and NH_3^+ or NH_4^+, which is similarly reported by Woo, Majid, and Arof (2011) and Selvasekarapandian, Baskaran, and Hema (2005) in their polymer-ammonium salt system. Nevertheless previous studies have reported only H^+ ion can contribute to the ionic transport (Samsudin et al., 2014). From Fig. 4**(a)**, peak at 1060 cm^{-1} denotes the C—O stretching of CH_2OH. The peak has shifted to 1059 cm^{-1}. This has been further validated by the calculated vibration frequency, where the C—O stretching for 2-HEC has been obtained at 1055 cm^{-1}, then slightly shifted to 1050 cm^{-1} for the complexes 2-HEC—NH_4NO_3. Since both experimental and computational results show very subtle changes, thus, confirmed that no interaction occurs in this region. New peak attributed to N—O stretching appeared at 826 cm^{-1} and 786 cm^{-1} for experimental and computational result respectively after addition of NH_4NO_3 salt, proving the presence of NH_4NO_3 salts in the polymer matrix.

Fig. 4**(b)** shows three peaks of C—H bending deformation (1457 cm^{-1}), C—O—H bending (1355 cm^{-1}) and C—O stretching (1249 cm^{-1}). It is noted that, the intensity of C—H and C—O—H bending significantly increased from 3.8% to 20.0% as presented in Fig. 6, and shifted to lower wavenumber of 1429 cm^{-1} and 1330 cm^{-1} upon addition of NH_4NO_3 composition. Meanwhile, the C—O stretching peak at 1249 cm^{-1} has disappeared. However, the shifting of C—H bending is less pronounces than that of the bending from hydroxyl group. These band apparently resulted from interaction between C—O—H bending of the hydroxyl end

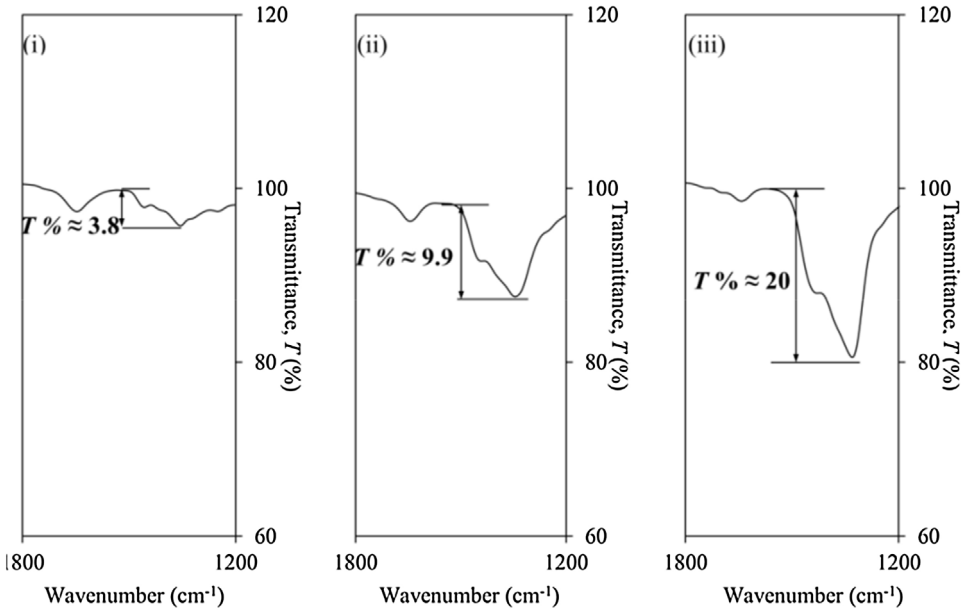

Fig. 6. The change in intensity of C—O—H bending for 2-HEC SPE with (i) 0-NH_4NO_3; (ii) 12-NH_4NO_3 and (iii) 24-NH_4NO_3 composition.

Table 3
FTIR vibration modes of 2-HEC powder and NH_4NO_3 salts.

Sample	Experimental ν (cm^{-1})	Calculation ν (cm^{-1}) Scaled[a]	Assignment	References
2-HEC powder	3387	3619–3475	ν(O—H) of alcohol	[1]
	2916 & 2878	2993–2782	ν_s(C—H) & ν_{as}(C—H) of alkane group	[2]
	1647	Not visible	naturally absorbed water	[3]
	1456	1460–1416	δ(C—H) deformation	[4]
	1354	1397–1182	δ(C—O—H) of alcohol	[5]
	1249 & 1053	1179–1082	ν(C—O)	[6]
	932,887&827	1079–573	ν(C—C) of glycosidic linkage	[7]
NH_4NO_3 salts	3250 & 3074	3434–2540	ν_{as}(N—H)	[8]
	1420	1603–1461	ν_{as}(N—O) & δ(N—H)	[9]
	1311	1296	ν_{as}(N—O)	[10]
	1043	1100–1068	ν_s(N—O)	[11]
	827	933	δ(N—O)	[12]

Number in references column represents the citation for each vibration mode presented in Table 3: [1] Abdel-Halim, 2014; Li, Wang, Wang, & Yu, 2014, [2] Azzaoui et al., 2015; Fadzallah et al., 2014, [3] Azzaoui et al., 2015; Diana Ciolacu et al., 2011, [4] Deyab, 2015; Shameli et al., 2012, [5] Deyab, 2015; Serrano, Marín, Gonzalo, & Labidi, 2012; Shameli et al., 2012), [6] Chen, Yi, Wu, & Guo, 2010, [7] Abdel-Halim, 2014; Kizil, Irudayaraj, & Seetharaman, 2002, [8] Kamarudin & Isa, 2013; Shukur et al., 2013, [9] Shuhaimi et al., 2009, [10] Kamarudin & Isa, 2013; Tanak & Marchewka, 2013, [11] Kamarudin & Isa, 2013; Shuhaimi et al., 2009; Tanak & Marchewka, 2013, [12] Shuhaimi et al., 2009; Tanak & Marchewka, 2013. ν_s – symmetric stretching, ν_{as} – asymmetric stretching, δ – bending vibration.

[a] Common scale factor of 0.95

Table 4
FTIR vibration modes of 2-HEC—NH_4NO_3 SPEs.

Experimental ν (cm^{-1})							Calculation (Scaled[a]) ν (cm^{-1})		Assignment
0-NH_4NO_3	4-NH_4NO_3	8-NH_4NO_3	12-NH_4NO_3	16-NH_4NO_3	20-NH_4NO_3	24-NH_4NO_3	2-HEC	2-HEC—NH_4NO_3 complex	
3403	3401	3400	3405	3393	3381	3407	3475	3451	ν(O—H)
–	–	3265	3251	3233	3230	3211	–	3145	ν_{as}(N—H)
–	–	–	–	3082	3094	3078	–	3025	ν_s(N—H)
2918	2918	2919	2922	2919	2919	2918	2937	2945	ν_{as}(C—H)
2880	2880	2880	2883	2884	2883	2886	2845	2841	ν_s(C—H)
–	–	–	–	–	2363	2362	–	2346	ν(N—H)
1457	1455	1446	1439	1437	1436	1429	1433	1422	δ(C— H)
1355	1354	1350	1345	1335	1333	1330	1289	1264	δ(C—O-H)
1249	1249	–	–	–	–	–	1080	1081	ν(C—O)
1060	1060	1059	1059	1059	1059	1059	1055	1050	ν(C—O)
–	–	825	826	826	827	827	–	786	ν(C—C), δ(N—O)

ν_s – symmetric stretching, ν_{as} – asymmetric stretching, δ – bending vibration.

[a] Common scale factor of 0.95

chain, which probably coordinated by NH_4^+ ion and consequently affecting the others band (Shukur & Kadir, 2014). The calculated vibration frequency of C—H bending deformation, C—O—H bending and C—O stretching for 2-HEC have been obtained at 1433 cm^{-1}, 1289 cm^{-1} and 1280 cm^{-1} respectively. The corresponding peaks have been shifted to 1422 cm^{-1}, 1264 cm^{-1} and 1081 cm^{-1} for 2-HEC—NH_4NO_3 complexes. The observed vibration positions were almost the same as reported by the previous work done by Monisha et al., (2017). This study certainly proved the interaction of 2-HEC—NH_4NO_3 SPE was occurred at the lone pair electron of oxygen atom from the end of hydrocarbon chain (C—O bond) of 2-HEC.

Referring to Fig. 4**(c)**, a broad absorption peak of O—H stretching at 3403 cm^{-1} has been shifted to higher wavenumber of 3407 cm^{-1}. Two new peaks of primary amine (N—H) were observed at 3251 cm^{-1} and 3082 cm^{-1} with addition of 12 wt.% NH_4NO_3, and shifted to 3211 cm^{-1} and 3078 cm^{-1} for 24 wt.% NH_4NO_3. From the calculated vibration frequency, the O—H stretching of 2-HEC has been obtained at 3475 cm^{-1} and shifted to 3451 cm^{-1} for 2-HEC—NH_4NO_3 complexes. Two new peaks were also identified at 3145 cm^{-1} and 3025 cm^{-1}, which respectively corresponds to asymmetrical and symmetrical N—H stretching from NH_4NO_3 salt. The emergence and shifting of N—H peak in the O—H region was inferred that complexation occurred between the lone pair of oxygen and H^+ ion from amine group (H—O···H—N—H_3), as elucidated in Fig. 4**(b)**. In tetrahedral structure of ammonium ion (NH_4^+), one of four hydrogen atom was loosely bounded to the nitrogen atom

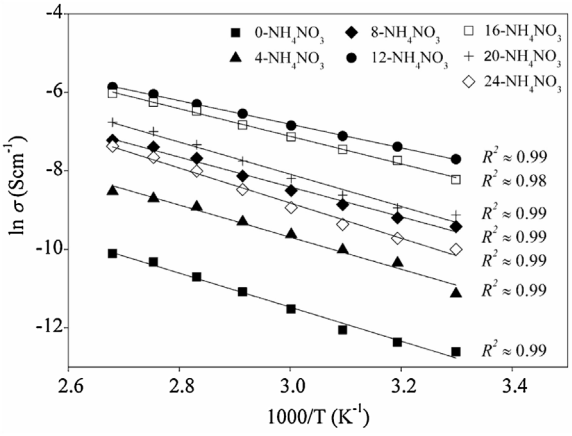

Fig. 7. Ionic conductivity at elevated temperature.

and can be easily dissociated under influence of an electric field. The protonated of H^+ ion for this system is following Grotthus mechanism where the ions migrated via hopping to the neighbouring vacant site (Ahmad & Isa, 2016; Hema et al., 2009; Sohaimy & Isa, 2016), hence, contributes to the conduction process. The proton transfer suggested in 2-HEC—NH_4NO_3 SPE is similar to that occurring in others proton conducting solid polymer electrolyte system reported by Ahmad and Isa (2016), Prokhorov et al. (2016),

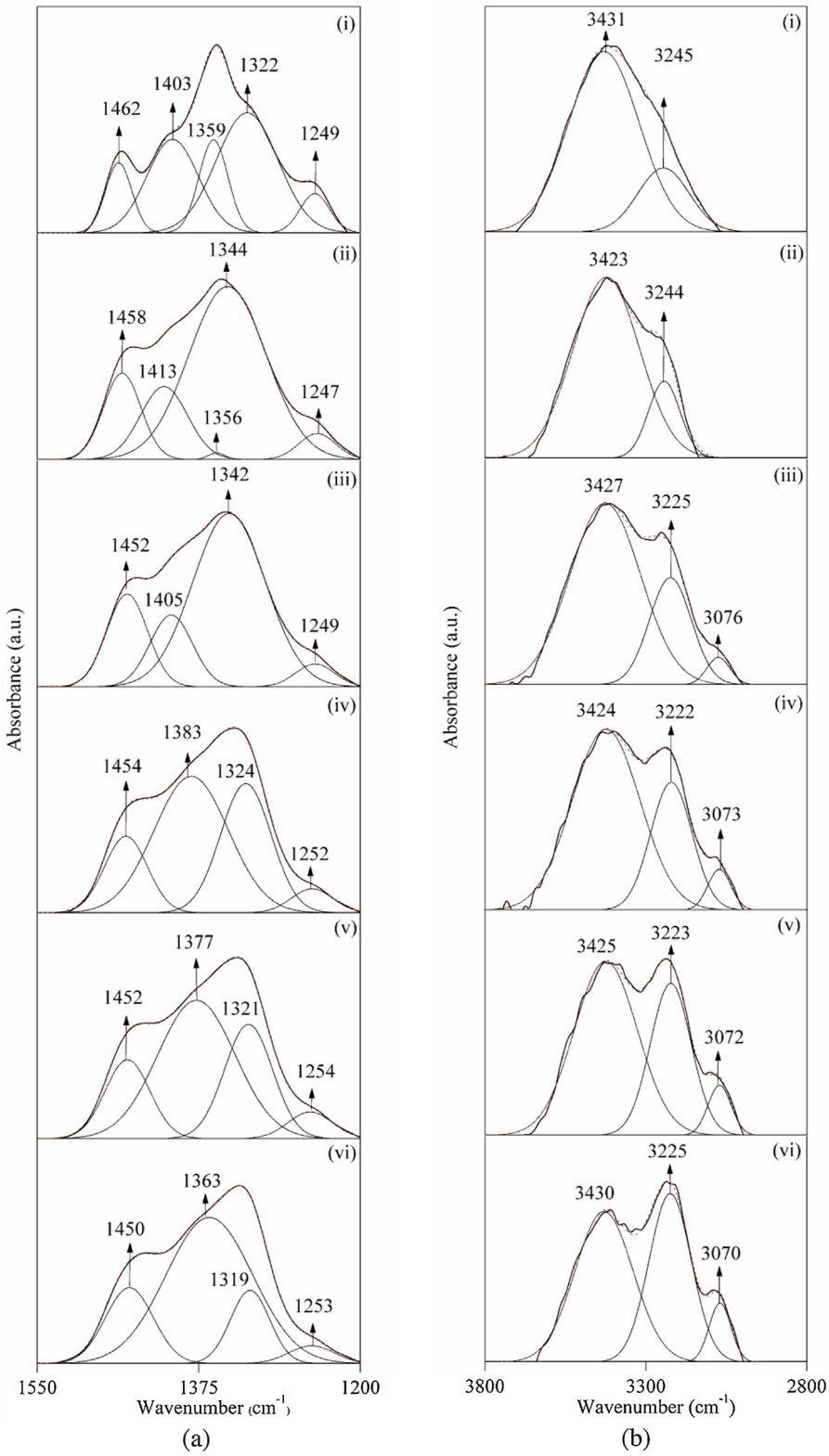

Fig. 8. Deconvoluted of IR spectrum in region (a) 1550–1200 cm^{-1}, (b) 3800–2800 cm^{-1} for 2-HEC SPE with (i) 4-NH_4NO_3; (ii) 8-NH_4NO_3; (iii) 12-NH_4NO_3; (iv) 16-NH_4NO_3; (v) 20-NH_4NO_3 and (vi) 24-NH_4NO_3 composition.

Meng et al. (2016). This interpretation, is the evidence of interaction occurred between 2-HEC and NH_4NO_3 of the SPE system. The bands assignment discussed in Fig. 4 are summarized in Table 4.

Additionally, the peak at 1647 cm^{-1} which corresponds to the naturally absorbed water was observed for all SPEs (Fig. 4**(b)**) (Azzaoui et al., 2015; Diana Ciolacu, Florin Ciolacu, & Popa, 2011). Since there is no obvious shifting upon addition of NH_4NO_3 salt, this study suggested no (or negligible) contribution of water content to the ionic conductivity of SPE. Nonetheless, in order to further ensure that there is no effect of water content towards ionic

conductivity enhancement, the SPEs were tested at elevated temperature. From Fig. 7, the increase of ionic conductivity with inverse temperature confirms that the SPEs obeys Arrhenius rule ($R^2 \sim 1$). No sudden drop or rise of ionic conductivity observed during the heating process proved that the ionic conductivity of SPE is not affected by water content, but it is due to the presence of charge carrier from the salt/ionic dopant (Sim et al., 2016).

Due to highly overlapping peak in Fig. 4**(b)** and **(c)**, the FTIR spectrum of the selected region were deconvoluted and plotted in Fig. 8. From Fig. 8**(a)**, the peak observed at 1462–1450 cm^{-1}, 1359–1356 cm^{-1} and 1254–1249 cm^{-1} correspond to C—H bending deformation, C—O—H bending mode and C—O stretching of 2-HEC, respectively. The C—O—H peak was disappeared after addition of 12 wt% NH_4NO_3. The characteristic band of N—O stretching was found at 1403–1363 cm^{-1} and 1319–1254 cm^{-1}. In Fig. 8**(b)**, the peak at 3431–3424 cm^{-1} and 3245–3222 cm^{-1} represent the O—H stretching of alcohol group from 2-HEC and N—H stretching from NH_4NO_3 salt, respectively. The emergence of new N—H peak was observed at 3075–3070 cm^{-1} after addition of 12 wt.% NH_4NO_3. The change in peak wavenumber, peak disappearing and emergence of new peak implies the complexes between 2-HEC and NH_4NO_3 salt. The peak obtained from IR deconvolution analysis is in agreement with the peak observed in Section 3.3.

4. Conclusion

A new solid polymer electrolyte (SPE) using of 2-hydroxyethyl cellulose (2-HEC) incorporated with different ammonium nitrate (NH_4NO_3) compositions was successfully prepared via solution casting method. The amorphous nature and interaction of 2-HEC—NH_4NO_3 SPE were explained using Fourier transform infrared (FTIR) spectroscopy and X-ray diffraction (XRD) to correlate the ionic conductivity of SPE. XRD analysis shows the most amorphous SPE was obtained for 2-HEC containing 12 wt.% of NH_4NO_3 composition with 95.65% of amorphous degree. A progressively increase in amorphous region provides more transit site for ion conduction. From FTIR analysis, 2-HEC SPE peaks (0-NH_4NO_3) at 3403 cm^{-1} correspond to O—H stretching of hydroxyl group and 1355 cm^{-1} correspond to C—O—H bending were examined and has been theoretically validated using Gaussian analysis software. In this study, the shifted peaks to lower wavenumber of C—O—H bending mode and new N—H peaks presence in O—H region with addition of NH_4NO_3 doping indicates that complexation occurred between the lone pair of oxygen and H^+ ion from amine group (H—O···H—N—H_3). All the information obtained from this study confirmed that the incorporation of NH_4NO_3 has enhanced the amorphousness of the SPE as well as endorse the complexation between the polymer chain and salt/doping materials. Furthermore, the increase of ion dissociated as the results of higher salt/dopant composition promotes more ion mobility through the polymer backbone, which in turn increases the ionic conductivity value.

Acknowledgements

The authors would like to acknowledge Ministry of Higher Education Malaysia (MOHE) and Universiti Malaysia Terengganu (UMT) for ERGS (vot. 55101) and FRGS (vot. 59452) grant, MyBrain15 for MyPhD awarded. Special thanks Advanced Materials Team, M.I.H. Sohaimy and M.N. Chai for the support given.

References

Abd El-kader, M. F. H., & Abu-Abdeen, M. (2012). Thermal and mechanical studies of PVP/2-HEC blend films. *Australian Journal of Basic and Applied Sciences*, *6*(13), 454–462.

Abdel-Halim, E. S. (2014). Chemical modification of cellulose extracted from sugarcane bagasse: Preparation of hydroxyethyl cellulose. *Arabian Journal of Chemistry*, *7*(3), 362–371.

Abdul Rahaman, M. H., Khandaker, M. U., Khan, Z. R., Kufian, M. Z., Noor, I. S., & Arof, A. K. (2014). Effect of gamma irradiation on poly(vinyledene difluoride)-lithium bis(oxalato)borate electrolyte. *Physical Chemistry Chemical Physics*, *16*(23), 11527–11537.

Ahmad, N. H., & Isa, M. I. N. (2016). Characterization of un-plasticized and propylene carbonate plasticized carboxymethyl cellulose doped ammonium chloride solid biopolymer electrolytes. *Carbohydrate Polymers*, *137*, 426–432.

Ali, A. M. M., Mohamed, N. S., & Arof, A. K. (1998). Polyethylene oxide (PEO)-ammonium sulfate ($(NH_4)_2SO_4$) complexes and electrochemical cell performance. *Journal of Power Sources*, *74*, 135–141.

Alias, S. S., Chee, S. M., & Mohamad, A. A. (2014). Chitosan-ammonium acetate-ethylene carbonate membrane for proton batteries. *Arabian Journal of Chemistry*, http://dx.doi.org/10.1016/j.arabjc.2014.05.001. In-press

Allen, G. (1986). Speciality polymers: Prospect – retrospect. *Materials & Design*, *7*(4), 179–181.

Amaral, F. A., Sousa, R. M., Morais, L. C. T., Rocha, R. G., Campos, I. O., Fagundes, W. S., & Canobre, S. C. (2015). Preparation and characterization of the porous solid polymer electrolyte of PAN/PVA by phase inversion. *Journal of Applied Electrochemistry*, *45*(8), 809–820.

Awadhia, A., & Agrawal, S. L. (2007). Structural, thermal and electrical characterizations of PVA:DMSO:NH_4SCN gel electrolytes. *Solid State Ionics*, *178*(13–14), 951–958.

Azzaoui, K., Mejdoubi, E., Lamhamdi, A., Zaoui, S., Berrabah, M., Elidrissi, A., & Al-Deyab, S. S. (2015). Structure and properties of hydroxyapatite/hydroxyethyl cellulose acetate composite films. *Carbohydrate Polymers*, *115*, 170–176.

Bakar, N. Y., Hafiza, M. N., Bashirah, A. N. A., & Isa, M. I. N. (2015). Electrical studies of carboxy methycellulose-chitosan blend biopolymer doped dodecyltrimethyl ammonium bromide solid electrolytes. *American Journal of Applied Sciences*, *12*(1), 40–46.

Byrne, N., Efthimiadis, J., MacFarlane, D. R., & Forsyth, M. (2004). The enhancement of lithium ion dissociation in polyelectrolyte gels on the addition of ceramic nano-fillers. *Journal of Materials Chemistry*, *14*(1), 127.

Chai, M. N., & Isa, M. I. N. (2016). Novel proton conducting solid bio-polymer electrolytes based on carboxymethyl cellulose doped with oleic acid and plasticized with glycerol. *Scientific Reports*, *6*, 27328.

Chen, R., Yi, C., Wu, H., & Guo, S. (2010). Degradation kinetics and molecular structure development of hydroxyethyl cellulose under the solid state mechanochemical treatment. *Carbohydrate Polymers*, *81*(2), 188–195.

Deyab, M. A. (2015). Hydroxyethyl cellulose as efficient organic inhibitor of zinc-carbon battery corrosion in ammonium chloride solution: electrochemical and surface morphology studies. *Journal of Power Sources*, *280*, 190–194.

Diana Ciolacu, Florin Ciolacu, & Popa, V. I. (2011). Amorphous cellulose-structure and characterization. *Cellulose Chemistry and Technology*, *45*(1–2), 13–21.

Eissa, A. M., Khosravi, E., & Cimecioglu, A. L. (2012). A versatile method for functionalization and grafting of 2-hydroxyethyl cellulose (HEC) via Click chemistry. *Carbohydrate Polymers*, *90*(2), 859–869.

Fadzallah, I. A., Majid, S. R., Careem, M. A., & Arof, A. K. (2014). A study on ionic interactions in chitosan–oxalic acid polymer electrolyte membranes. *Journal of Membrane Science*, *463*, 65–72.

Hafiza, M. N., & Isa, M. I. N. (2014). Ionic conductivity and conduction mechanism studies of CMC/Chitosan biopolymer blend electrolytes. *Research Journal of Recent Sciences*, *3*(11), 50–56.

Hafiza, M. N., Bashirah, A. N. A., Bakar, N. Y., & Isa, M. I. N. (2014). Electrical properties of carboxyl methylcellulose/chitosan dual-blend green polymer doped with ammonium bromide. *International Journal of Polymer Analysis and Characterization*, *19*(2), 151–158.

Hema, M., Selvasekarapandian, S., Arunkumar, D., Sakunthala, A., & Nithya, H. (2009). FTIR, XRD and ac impedance spectroscopic study on PVA based polymer electrolyte doped with NH_4X (XCl, Br, I). *Journal of Non-Crystalline Solids*, *355*(2), 84–90.

Hodge, R. M., Edward, G. H., & Simon, G. P. (1996). Water absorption and states of water in semicrystalline poly(vinyl alcohol) films. *Polymer*, *37*(8), 1371–1376.

Ibrahim, S., Yassin, M. M., Ahmad, R., & Johan, M. R. (2011). Effects of various $LiPF_6$ salt concentrations on PEO-based solid polymer electrolytes. *Ionics*, *17*(5), 399–405.

Isa, M. I. N., & Samsudin, A. S. (2016). Potential study of biopolymer-based carboxymethylcellulose electrolytes system for solid-state battery application. *International Journal of Polymeric Materials and Polymeric Biomaterials*, *65*(11), 561–567.

Kamarudin, K. H., & Isa, M. I. N. (2013). Structural and DC Ionic conductivity studies of carboxymethylcellulose doped with ammonium nitrate as solid polymer electrolytes. *International Journal of Physical Sciences*, *8*(31), 1581–1587.

Kizil, R., Irudayaraj, J., & Seetharaman, K. (2002). Characterization of irradiated starches by using FT-Raman and FTIR spectroscopy. *Journal of Agricultural and Food Chemistry*, *50*(14), 3912–3918.

Li, F., Wang, W., Wang, X., & Yu, J. (2014). Changes of structure and property of alkali soluble hydroxyethyl celluloses (HECs) and their regenerated films with the molar substitution. *Carbohydrate Polymers*, *114*, 206–212.

Liew, C. W., & Ramesh, S. (2015). Electrical, structural: thermal and electrochemical properties of corn starch-based biopolymer electrolytes. *Carbohydrate Polymers*, *124*, 222–228.

Meng, T., Young, K., Beglau, D., Yan, S., Zeng, P., & Cheng, M. M.-C. (2016). Hydrogenated amorphous silicon thin film anode for proton conducting batteries. *Journal of Power Sources*, *302*, 31–38.
Miao, X., Lin, J., Tian, F., Li, X., Bian, F., & Wang, J. (2016). Cellulose nanofibrils extracted from the byproduct of cotton plant. *Carbohydrate Polymers*, *136*, 841–850.
Monisha, S., Mathavan, T., Selvasekarapandian, S., Milton Franklin Benial, A., Aristatil, G., Mani, N., & Vinoth Pandi, D. (2017). Investigation of bio polymer electrolyte based on cellulose acetate-ammonium nitrate for potential use in electrochemical devices. *Carbohydrate Polymers*, *157*, 38–47.
Murata, K., Izuchi, S., & Yoshihisa, Y. (2000). An overview of the research and development of solid polymer electrolyte batteries. *Electrochimica Acta*, *45*(8–9), 1501–1508.
Murata, K. (1995). An overview of the research and development of solid polymer electrolyte batteries. *Electrochimica Acta*, *40*(13–14), 2177–2184.
Pawlicka, A., Sabadini, A. C., Raphael, E., & Dragunski, D. C. (2008). Ionic conductivity thermogravimetry measurements of starch-based polymeric electrolytes. *Molecular Crystals and Liquid Crystals*, *485*(1), 804–816.
Pethrick, R. A. (1986). The development and application of polymeric materials for the electronics industry. *Materials & Design*, *7*(4), 173–178.
Poiyamozhi, A., Sundaraganesan, N., Karabacak, M., Tanrıverdi, O., & Kurt, M. (2012). The spectroscopic (FTIR, FT-Raman, UV and NMR), first-order hyperpolarizability and HOMO-LUMO analysis of 4-amino-5-chloro-2-methoxybenzoic acid. *Journal of Molecular Structure*, *1024*, 1–12.
Prokhorov, E., Luna-Bárcenas, G., González-Campos, J. B., Kovalenko, Y., García-Carvajal, Z. Y., & Mota-Morales, J. (2016). Proton conductivity and relaxation properties of chitosan-acetate films. *Electrochimica Acta*, *215*, 600–608.
Przyłuski, J., & Wieczorek, W. (1989). Increasing the conductivity of polymer solid electrolytes: A review. *Solid State Ionics*, *36*(3–4), 165–169.
Qiu, X., & Hu, S. (2013). Smart materials based on cellulose: A review of the preparations, properties, and applications. *Materials*, *6*(3), 738–781.
Radha, K. P., Selvasekarapandian, S., Karthikeyan, S., Hema, M., & Sanjeeviraja, C. (2013). Synthesis and impedance analysis of proton-conducting polymer electrolyte PVA:NH_4F. *Ionics*, *19*(10), 1437–1447.
Ramesh, S., Shanti, R., & Morris, E. (2013). Characterization of conducting cellulose acetate based polymer electrolytes doped with green ionic mixture. *Carbohydrate Polymers*, *91*(1), 14–21.
Ramlli, M. A., & Isa, M. I. (2016). Structural and ionic transport properties of protonic conducting solid biopolymer electrolytes based on carboxymethyl cellulose doped with ammonium fluoride. *The Journal of Physical Chemistry B*, *120*(44), 11567–11573.
Rudhziah, S., Rani, M. S. A., Ahmad, A., Mohamed, N. S., & Kaddami, H. (2015). Potential of blend of kappa-carrageenan and cellulose derivatives for green polymer electrolyte application. *Industrial Crops and Products*, *72*, 133–141.
Salleh, N. S., Aziz, S. B., Aspanut, Z., & Kadir, M. F. Z. (2016). Electrical impedance and conduction mechanism analysis of biopolymer electrolytes based on methyl cellulose doped with ammonium iodide. *Ionics*, *22*(11), 2157–2167.
Samsudin, A. S., & Isa, M. I. N. (2014). Study of the ionic conduction mechanism based on carboxymethyl cellulose biopolymer electrolytes. *Journal of the Korean Physical Society*, *65*(9), 1441–1447.
Samsudin, A. S., Khairul, W. M., & Isa, M. I. N. (2012). Characterization on the potential of carboxy methylcellulose for application as proton conducting biopolymer electrolytes. *Journal of Non-Crystalline Solids*, *358*(8), 1104–1112.
Samsudin, A. S., Lai, H. M., & Isa, M. I. N. (2014). Biopolymer materials based carboxymethyl cellulose as a proton conducting biopolymer electrolyte for application in rechargeable proton battery. *Electrochimica Acta*, *129*, 1–13.
Selvasekarapandian, S., Baskaran, R., & Hema, M. (2005). Complex AC impedance, transference number and vibrational spectroscopy studies of proton conducting PVAc-NH_4SCN polymer electrolytes. *Physica B: Condensed Matter*, *357*(3–4), 412–419.
Selvasekarapandian, S., Hema, M., Kawamura, J., Kamishima, O., & Baskaran, R. (2010). Characterization of PVA-NH_4NO_3 polymer electrolyte and its application in rechargeable proton battery. *Journal of the Physical Society of Japan*, *79*(suppl A), 163–168.
Serrano, L., Marín, F., Gonzalo, A., & Labidi, J. (2012). Integral use of pepper stems. *Industrial Crops and Products*, *40*, 110–115.
Shameli, K., Ahmad, M. B., Jazayeri, S. D., Sedaghat, S., Shabanzadeh, P., Jahangirian, H., & Abdollahi, Y. (2012). Synthesis and characterization of polyethylene glycol mediated silver nanoparticles by the green method. *International Journal of Molecular Sciences*, *13*(6), 6639–6650.
Shuhaimi, N. E. A., Majid, S. R., & Arof, A. K. (2009). On complexation between methyl cellulose and ammonium nitrate. *Materials Research Innovations*, *13*(3), 239–242.
Shukur, M. F., & Kadir, M. F. Z. (2014). Electrical and transport properties of NH_4Br-doped cornstarch-based solid biopolymer electrolyte. *Ionics*, *21*(1), 111–124.
Shukur, M. F., & Kadir, M. F. Z. (2015). Hydrogen ion conducting starch-chitosan blend based electrolyte for application in electrochemical devices. *Electrochimica Acta*, *158*, 152–165.
Shukur, M. F., Ithnin, R., Illias, H. A., & Kadir, M. F. Z. (2013). Proton conducting polymer electrolyte based on plasticized chitosan-PEO blend and application in electrochemical devices. *Optical Materials*, *35*(10), 1834–1841.
Silverstein, R. M., Webster, F. X., & Kiemle, D. (2005). *Spectrometric identification of organic compounds*. John Wiley & Sons Inc.
Sim, L. N., Yahya, R., & Arof, A. K. (2016). Blend polymer electrolyte films based on poly(ethyl methacrylate)/poly(vinylidenefluoride-co-hexafluoropropylene) incorporated with 1-butyl-3-methyl imidazolium iodide ionic liquid. *Solid State Ionics*, *291*, 26–32.
Singh, R., Jadhav, N. A., Majumder, S., Bhattacharya, B., & Singh, P. K. (2013). Novel biopolymer gel electrolyte for dye-sensitized solar cell application. *Carbohydrate Polymers*, *91*(2), 682–685.
Sohaimy, M. I. H., & Isa, M. I. N. (2016). Ionic conductivity and conduction mechanism studies on cellulose based solid polymer electrolytes doped with ammonium carbonate. *Polymer Bulletin*, http://dx.doi.org/10.1007/s00289-016-1781-5. In-press
Sudaryanto, Yulianti, E., & Patimatuzzohrah. (2016). Structure and properties of solid polymer electrolyte based on chitosan and ZrO_2 nanoparticle for lithium ion battery. *AIP Conference Proceeding*, *1710*, 020003–020009.
Taghizadeh, M. T., & Seifi-Aghjekohal, P. (2015). Sonocatalytic degradation of 2-hydroxyethyl cellulose in the presence of some nanoparticles. *Ultrasonics Sonochemistry*, *26*, 265–272.
Tanak, H., & Marchewka, M. K. (2013). FT-IR, FT-Raman, and DFT computational studies of melaminium nitrate molecular-ionic crystal. *Journal of Molecular Structure*, *1034*, 363–373.
Trivedi, M. K., Nayak, G., Patil, S., Tallapragada, R. M., & Mishra, R. (2015). Influence of biofield treatment on physicochemical properties of hydroxyethyl cellulose and hydroxypropyl cellulose. *Journal of Molecular Pharmaceutics & Organic Process Research*, *03*(02).
Voigt, N., & van Wüllen, L. (2012). The mechanism of ionic transport in PAN-based solid polymer electrolytes. *Solid State Ionics*, *208*, 8–16.
Woo, H. J., Majid, S. R., & Arof, A. K. (2011). Conduction and thermal properties of a proton conducting polymer electrolyte based on poly (ε-caprolactone). *Solid State Ionics*, *199–200*, 14–20.